Research Square

Preprints are preliminary reports that have not undergone peer review.
They should not be considered conclusive, used to inform clinical practice,
or referenced by the media as validated information.

Background parenchymal enhancement (BPE) and tumor contrast on photon-counting CT (PC-CT) with dedicated breast reconstructions: comparison with breast MRI

Caroline Wilpert

caroline.wilpert@uniklinik-freiburg.de

University Medical Center Freiburg

Lisa Jung

University Medical Center Freiburg

Robin Johannes Antonius Duteweert

Rijnstate Hospital

Carla Meeuwis

Rijnstate Hospital

Monique Dorrius

University Medical Center Groningen

Stephan Rau

University Medical Center Freiburg

Jakob Weiss

University Medical Center Freiburg

Ingolf Juhasz-Böss

University Medical Center Freiburg

Marisa Windfuhr-Blum

University Medical Center Freiburg

Fabian Bamberg

University Medical Center Freiburg

Jakob Neubauer

University Medical Center Freiburg

Research Article

Keywords: Breast Density, Breast Neoplasms, Contrast Media, Dynamic Contrast Enhanced Magnetic Resonance Imaging, Tomography, X-Ray Computed

Posted Date: November 18th, 2026

DOI: https://doi.org/10.21203/rs.3.rs-11592176/v1

License: This work is licensed under a Creative Commons Attribution 4.0 International License.
Read Full License

Additional Declarations: No competing interests reported.

Background parenchymal enhancement (BPE) and tumor contrast on photon-counting CT (PC-CT) with dedicated breast reconstructions: comparison with breast MRI

Original Research

Authors

Caroline Wilpert[1], Lisa Jung[2], Robin Johannes Antonius Duteweert[3,4], Carla Meeuwis[3], Monique Dorrius[4], Stephan Rau[1], Jakob Weiss[1], Ingolf Juhasz-Böss[2], Marisa Windfuhr-Blum[1], Fabian Bamberg[1], Jakob Neubauer[1]

Affiliations:

[1] Department of Diagnostic and Interventional Radiology, Medical Center, University of Freiburg, Faculty of Medicine, University of Freiburg, Hugstetterstr. 55, 79106 Freiburg, Germany
[2] Department of Obstetrics and Gynecology at the Medical Center, University of Freiburg, Hugstetterstr. 55, 79106 Freiburg, Germany
[3] Rijnstate Hospital Arnhem, Department of Radiology & Nuclear Medicine, Arnhem, Wagnerlaan 55, Arnhem, 6815AD, The Netherlands
[4] University of Groningen, University Medical Center Groningen, Department of Radiology, Groningen, PO Box 30.001, EB44, Groningen, 9700 RB, The Netherlands

Corresponding author:
Caroline Wilpert, M.D.
Department of Diagnostic and Interventional Radiology,
Medical Center, University of Freiburg
Hugstetterstr. 55
79106 Freiburg – Germany
Email: caroline.wilpert@uniklinik-freiburg.de
Phone: 0049-761-270-38190

Manuscript type: Original Article

Word count:
Abstract: 282
Main Document: 4655
Number of Figures: 4
Number of Tables: 5
Number of Supplemental Tables: 4
Number of Supplemental Figures: 1

Data generated or analyzed during the study are available from the corresponding author on reasonable request.

Title

Background parenchymal enhancement (BPE) and tumor contrast on photon-counting CT (PC-CT) with dedicated breast reconstructions: comparison with breast MRI

Original research article

Abstract

Background

Background parenchymal enhancement (BPE) can obscure breast cancers in contrast-enhanced imaging. We compared BPE, lesion contrast, and lesion-size estimates on prone photon-counting CT (PC-CT) compared with breast MRI.

Methods

This retrospective single-center study included patients with biopsy-proven breast cancer who underwent same-day prone contrast-enhanced PC-CT and breast MRI. PC-CT reconstructions comprised iodine maps and monoenergetic post-contrast images. Malignant lesion contrast-to-noise ratios (CNRs), diameters, BPE characteristics, T-category, and ductal carcinoma in situ (DCIS) suspicion were assessed. Interreader reliability was evaluated using weighted Cohen's kappa.

Results

Thirty-two patients were included (mean age 53 ± 14 years). Tumor-to-parenchyma CNR was numerically higher on MRI ($p = 0.138$) and tumor-to-fat CNR on PC-CT ($p = 0.165$), without significant differences. MRI yielded larger long-axis tumor diameters than PC-CT (31.3 ± 21.4 mm versus 29.5 ± 21.2 mm, $p = 0.005$), whereas short-axis diameter did not differ ($p = 0.420$). Five of 31 lesions (16%) shifted by one adjacent size category, MRI assigned a larger category in four cases. Imaging-based T-category was identical between modalities for both readers. Median BPE intensity was significantly lower on PC-CT iodine maps than on MRI for both readers (R1: 1 [IQR 1–2], R2: 1 [IQR 1–2] vs. R1: 2 [1–3], R2: 2 [2–3]; $p < 0.001$). Interreader agreement was substantial for BPE intensity on PC-CT iodine maps ($\kappa = 0.669$) and MRI ($\kappa = 0.773$) and almost perfect for DCIS-suspicion ratings ($\kappa = 0.851$). Both readers considered BPE to be best depicted on iodine maps in 32/32 cases.

Conclusions

In this small retrospective cohort, prone contrast-enhanced PC-CT showed lower BPE than MRI, while lesion contrast remained comparable. MRI yielded larger long-axis measurements, while imaging-based T-category remained identical. DCIS related observations remain exploratory and require validation.

Keywords: Breast Density; Breast Neoplasms; Contrast Media; Dynamic Contrast Enhanced Magnetic Resonance Imaging; Tomography, X-Ray Computed

Background

Background parenchymal enhancement (BPE), defined as physiological enhancement of fibroglandular breast tissue, is a known phenomenon in breast magnetic resonance imaging (MRI) (1) and contrast-enhanced spectral mammography (CESM) (2, 3) reflecting hormonal and vascular responsiveness of the breast parenchyma (4, 5). BPE is independent of breast density (6), but varies with hormonal influences (7), typically appears symmetrically (8), and fluctuates across the menstrual cycle (9), with lowest levels in the second week (10, 11). Higher BPE is commonly observed in premenopausal women (4, 7, 11), during lactation, and under hormone therapy (12), including intrauterine hormonal devices (13), and decreases after endocrine (14, 15), cytotoxic (4, 16, 17) or radiation therapy (18, 19). Moderate and marked BPE remains a limitation of breast MRI, as it may obscure lesions, increases abnormal interpretation rates, recall and biopsy rates (18, 20) and reduces sensitivity and specificity (21, 22). Strong BPE, particularly larger focal areas of BPE, can be a challenge for the detection of non-mass enhancing lesions such as ductal carcinoma in situ (DCIS) (8, 23).

Beyond its limiting effect on diagnostic interpretation in breast MRI, BPE has emerged as an independent functional imaging biomarker of clinical relevance (1, 24). Strong BPE levels are associated with an increased breast cancer risk of around 2-10-fold across multiple cohorts (1, 25-31). Furthermore, a reduction of BPE during neoadjuvant chemotherapy has been correlated with pathological complete response, highlighting its potential as a predictive marker of treatment efficacy (19).

While BPE has been extensively characterized in MRI and, more recently, in CESM (2, 3, 12), its appearance in CT-based breast imaging remains poorly understood.

A recent comparative study reported substantial agreement for BPE assessment and lower BPE level between contrast-enhanced (CE) cone-beam breast CT (CB-BCT) and MRI (32), suggesting potentially lower masking. Photon-counting CT (PC-CT), with its improved spatial resolution, contrast-to-noise ratio (CNR) and spectral imaging capability (33, 34), may further advance CT-based breast assessment, particularly when combined with prone positioning and iodine mapping for quantification of vascularity. However, a systematic investigation of BPE in PC-CT is still lacking.

Therefore, the aim of this study was to intra-individually compare the appearance and intensity of BPE on prone PC-CT using dedicated breast reconstructions derived from a thoracoabdominal acquisition with same-day breast MRI and to compare lesion CNR and tumor-size estimates. Imaging based T-category concordance and suspicion of associated DCIS were evaluated as exploratory secondary observations.

Methods

Study cohort

This retrospective single-center study was approved by the Ethics Committee of the Albert-Ludwigs-University of Freiburg, Medical Center – University of Freiburg, Faculty of Medicine, Freiburg, Germany (approval reference: EK24-1487-S1-retro; FRKS005501, retrospective). Written informed consent was not required because of the retrospective study design. The study was registered in the German Clinical Trials Register (DRKS00035784) on 20. December 2024 and is in line with the Declarations of Helsinki. Consecutive patients with biopsy-proven breast cancer who underwent same-day prone PC-CT and breast MRI between November 2021 and August 2023 for staging reasons were included. MRI served as comparative standard for BPE and DCIS suspicion. Mammography/tomosynthesis within ≤50 days was used for breast density reference. Initial biopsy reports served as the reference for histology and immunohistochemical tumor characteristics. Most specimens were evaluated at the Department of Pathology, University Medical Center Freiburg; external reports were used when biopsy or surgery had been performed elsewhere. Within the routine clinical pathology workflow, pretreatment core-biopsy reports did not consistently include a separate nuclear grade in case of associated DCIS components, particularly when the biopsy had established invasive carcinoma. This information could therefore not be reconstructed reliably in retrospect. ER/PR positivity, PR level, Ki-67, HER2 status, and surrogate subtype were classified using the predefined thresholds summarized in Table 2. Surrogate subtypes were assigned as Luminal A-like, Luminal B-like HER2-negative/low, Luminal B-like HER2-positive, HER2-enriched, or triple-negative according to ER, PR, HER2, and Ki-67 status. Twenty-four of 32 patients initiated neoadjuvant systemic therapy after the same-day PC-CT and MRI examinations and before surgery, whereas 8/32 underwent upfront surgery. The examinations evaluated in this study therefore represented pretreatment baseline imaging. Because surgical pathological T category represented residual post-treatment disease in most patients, it was not used as a uniform reference standard for baseline imaging tumor extent. Therefore imaging-based T-category assessment was analyzed as paired inter-modality concordance between PC-CT and MRI. Exclusion criteria were lack of same-day diagnostic MRI and PC-CT, non-diagnostic imaging quality, absence of pathological confirmation or malignancy or of pathological data required for the prespecified primary analyses, and recent breast surgery. Unavailable ancillary variables not required for eligibility or the primary analyses, including a separately reported

nuclear grade of an associated DCIS component, were recorded as missing and did not lead to exclusion. Endocrine therapy or medication intake was not an exclusion criterion.

Imaging protocol

PC-CT was performed on a first-generation system (NAEOTOM Alpha, Siemens Healthineers) using dual-source, multi-energy thoracoabdominal protocols (120 kV, automated tube current, 142 mAs). Weight-adjusted iopromide (370 mg I/mL) was administered at 3 mL/s, and image acquisition was initiated 85 seconds after contrast injection. Examinations were performed in prone position using a free-hanging breast protocol (35). Axial dedicated breast CT reconstructions (Field of view: 34 cm, matrix: 1024x1024; 2 mm slice thickness/increment; Br40 kernel, iterative strength: 3, in-plane spatial resolution: 0.3x0.3x2.0 mm) included photon-counting CT iodine-map reconstruction (PC-CT_{Iodine}) and 65-keV monoenergetic post-contrast reconstructions (PC-CT_{C+}). Radiation exposure was taken from the CT scanner output protocol.

Breast MRI was performed on a 3T MRI system (MAGNETOM Vida, Siemens Healthineers) using an 18-channel breast coil with a standardized multiparametric breast MRI protocol including a T2-weighted Dixon imaging and dynamic contrast-enhanced T1-weighted Dixon/VIBE imaging acquired before and after intravenous administration of gadoteridol (ProHance, Bracco Imaging) at a dose of 0.1 mmol/kg body weight and an injection rate of 2.5 mL/s. For quantitative lesion assessment and BPE evaluation, the early post-contrast subtraction images of the dynamic T1-weighted Dixon/VIBE sequence and maximum intensity projections were used. The first post-contrast T1-weighted/VIBE acquisition, obtained approximately 90 seconds after contrast gadoteridol injection, was used for measurements and BPE measurement. This sequence was selected because early post-contrast imaging best reflects initial lesion enhancement and is time-sensitive for BPE assessment. In addition, the timing closely matched the PC-CT acquisition initiated 85 seconds after contrast injection. Digital breast tomosynthesis/mammography was used for breast density assessment.

Quantitative assessment of lesion contrast and tumor diameter

Quantitative analyses were patient-based and used one prespecified target lesion per patient. In unilateral multifocal or multicentric disease, the largest measurable malignant lesion in the affected breast was selected. Circular regions of interests were independently placed in the quantitative target lesion, in representative

enhancing fibroglandular tissue, and fat by one reader on matched axial post-contrast image series for each modality, using iodine maps for PC-CT and early-phase subtraction images of the T1-weighted Dixon VIBE sequence for MRI. Tumor ROIs (mean = μ) were positioned in the largest visible enhancing tumor lesion, preferably within the solid tumor component showing maximum enhancement, while avoiding necrosis, clip markers, partial-volume effects, vessels and adjacent DCIS-like enhancement. ROI size was adapted to tumor size. Reference ROIs in fibroglandular tissue and fat were adjusted according to breast size and tissue configuration to represent reproducible breast tissue for each case, while avoiding vessels, focal enhancement, and artifacts. Tumor-to-parenchyma and tumor-to-fat CNRs were calculated as follows:

$$\mathrm{CNR}_{\mathrm{Tumor-to-Parenchyma}} = (\mu\mathrm{Tumor} - \mu\mathrm{Parenchyma}) \Big/ \sqrt{\left(\left(SD^2{}_{\mathrm{Tumor}} + SD^2{}_{\mathrm{Parenchyma}}\right)/2\right)}$$

$$\mathrm{CNR}_{\mathrm{Tumor-to-Fat}} = (\mu\mathrm{Tumor} - \mu\mathrm{Fat}) \Big/ \sqrt{\left(\left(SD^2{}_{\mathrm{Tumor}} + SD^2{}_{\mathrm{Fat}}\right)/2\right)}$$

Noise was estimated as the mean standard deviation (SD) of tumor and reference tissue to account for local heterogeneity across reconstructions. Largest tumor diameters were measured on post-contrast axial images of both modalities. Adjacent DCIS was not assessed quantitatively. Target lesion ROI area ranged from 3 to 203 mm², with a median of 25 mm², corresponding to an equivalent median circular diameter of 5.6 mm. Median fibroglandular-tissue ROI area was 36 mm² (median diameter: 6.8 mm), and median fat ROI area was 65 mm² (median diameter: 9.1 mm). Representative ROI placements for PC-CT are provided in Supplemental Figure 1. Tumors were handled as target lesions and measured quantitatively. Cases with pure DCIS were excluded from the quantitative analysis. Axial tumor size was recorded as the longest tumor diameter and the perpendicular short-axis diameter in millimeters on matched post-contrast axial images of both modalities. The analysis was performed for the target lesion in each patient. In addition, an axial area product was calculated as longest diameter × short-axis diameter. Paired modality differences were calculated as MRI minus PC-CT.

Qualitative assessment of BPE, T-stages, DCIS suspicion and preferred image reconstruction type

Two experienced radiologists (13 years and 6 years in breast imaging) independently rated BPE intensity on an ordinal scale adapted from the Breast Imaging Reporting and Data System (BI-RADS) (1 = minimal, 2 = mild, 3 = moderate, 4 = marked) randomized for patient and modality on diagnostic monitors (36). For PC-CT, these categories constituted a study-specific ordinal comparative score adapted from the MRI BI-RADS categories. The score was used solely for intraindividual research comparison and should not be interpreted as a proposed or validated PC-CT classification. Readers assigned imaging T-category for PC-CT and MRI, noted DCIS suspicion (no/yes/associated), and recorded the preferred reconstruction type for BPE assessment on PC-CT (1=PC-CT_{C+}, 2=PC-CT_{Iodine}, 3=similar). DCIS suspicion was defined as a reader-recorded imaging impression, was evaluated only as an exploratory descriptive variable and it was not considered a diagnosis of DCIS or a measure of diagnostic performance. Subgroup analysis was performed for the groups low BPE (minimal and mild) vs. higher BPE ratings (moderate and marked). Breast density was extracted from mammography reports and pathological tumor characteristics from clinical reports. Readers were blinded to pathology results and detailed clinical information, including information on associated DCIS, but were aware that all patients had biopsy-proven breast cancer.

Statistical analysis

Continuous variables are presented as mean ± SD for normally distributed data or as median with interquartile range [IQR] for non-normally distributed data. Categorical variables are expressed as counts and percentages. Depending on data distribution, paired two-sided t-tests (quantitative analysis), Wilcoxon signed-rank tests (qualitative analysis), Friedman (BPE intensity subgroup analysis) and Welch's two-sample t-test (breast density subgroup analysis), were applied as appropriate. An exploratory stratified analysis was performed in women classified as premenopausal or postmenopausal to assess whether the direction of paired intermodal BPE difference was consistent across menopausal status. The perimenopausal participant and the participant with unknown menopausal status were excluded from the analysis. Because the study was not powered to test effect modification, the findings were summarized descriptively using medians and IQRs. Overall interreader agreement was assessed using linear-weighted Cohen's κ (37). As an exploratory category-level analysis, category-specific positive agreement was calculated separately for PC-CT iodine maps and MRI. Within each reader, assignment of each BPE category on PC-CT iodine maps versus MRI was compared using exact McNemar tests after dichotomization as the respective category versus all other categories, p values were Holm-

adjusted across the four category-specific comparisons. For the additional tumor-size analysis, mean, standard deviation, 95% confidence interval, median, and interquartile range were calculated for the long-axis diameter, short-axis diameter, and axial area product. Paired comparisons between MRI and PC-CT were performed using paired t-tests when paired differences were normally distributed and Wilcoxon signed-rank tests otherwise. A two-sided p-value < 0.05 was considered statistically significant. All analyses were performed using SPSS v30.0 (IBM Corp., Armonk, NY, USA).

Results

Patient cohort

Thirty-two patients (mean age of 53 ± 14 SD years, 31 women) were included. Of 602 screened participants, 78 had completed breast MRI and PC-CT; 46 were excluded because examinations were not performed on the same-day, resulting in the final cohort of 32 patients. Breast MRI served as comparative modality for BPE and tomosynthesis/mammography for breast density (Figure 1).

Patient and lesion characteristics

Fourteen of 32 participants were premenopausal, 1/32 (3%) perimenopausal (defined by gradually increasing fluctuation of symptoms with irregular menstrual cycle) and 16/32 (50%) postmenopausal. For 1/32 (3%) male participant menopausal status was not applicable. 1/32 (3%) reported intake of oral contraception. At the time of imaging 2/32 (6%) reported ongoing adjuvant endocrine therapy with tamoxifen after completion of primary breast cancer treatment. As tamoxifen may reduce BPE, its use was recorded and is acknowledged as a potential confounder. Neither patient had received chemotherapy, radiotherapy, surgery, or other cancer-directed treatment for the lesion evaluated in the present study before same-day examinations. Breast density was BI-RADS A in 3/32 (9%), B in 10/32 (31%), C in 8/32 (25%) and D in 11/32 (34%) cases; no silicone implants were present (Table 1).

Histology comprised 22/32 (69%) invasive carcinoma of no special type, 7/32 (22%) invasive carcinoma of no special type with associated DCIS, 2/32 (6%) invasive lobular carcinoma, and 1/32 (3%) pure DCIS. A separate nuclear grade for the associated DCIS component was documented in 4/7 cases 1/7 low-grade, 1/7 intermediate-grade, 2/7 high-grade and was unavailable in 3/7 cases. The nuclear grade of the single pure DCIS case was high. Among the 31 invasive carcinomas, 5 (16%) were luminal A-like, 10 (32%) luminal B-like (HER2-negative), 7 (23%) luminal B-like (HER2-positive), 5 (16%) HER2-enriched, and 4 (13%) triple-negative. The cohort comprised 29 patients with unilateral unifocal disease, 2 with unilateral multifocal or multicentric disease, and one patient with bilateral breast cancers. Imaging-based T category was assigned for the largest diameter cancer in the bilateral case. Tumors were right-sided in 15/32 (47%), left-sided in 16/32 (50%), and bilateral in 1/32

(3%). Most tumors were cT1 7/32 (22%) [cT1a: 2/32, cT1b: 1/32, cT1c: 4/32] or cT2: 13/32 (41%). 4/32 (13%) were cT3, 7/32 (22%) were cT4 and 1/32 (3%) was Tis. 12/32 (38%) had clinically node-positive disease. 2/32 (6%) had metastatic disease (Table 2).

Radiation exposure

Radiation dose of the entire thoracoabdominal volume was within standard-of-care limits (Dose-length product (DLP) = 803 ± 336 mGy·cm; CT Dose volume index ($CTDI_{vol}$) = 12 ± 5 mGy). Five examinations with $CTDI_{vol}$ above 18 mGy were observed in patients with elevated body mass index (30-41 kg/m²).

CNR

Mean tumor-to-parenchyma CNR was higher on MRI than PC-CT (6.7 ± 4.2 (95%-CI: [5.2; 8.3]) vs. 5.7 ± 3.6 (95%-CI [4.4; 7.0]); p = 0.138) and mean tumor-to-fat CNR was higher in PC-CT compared to MRI (12.0 ± 4.7 (95%-CI [10.3; 13.7]) vs. 10.4 ± 4.9 (95%-CI [8.6; 12.2]); p = 0.165); however, neither difference reached statistical significance (Figure 2). When stratified by breast density, pooled BI-RADS A/B categories showed numerically higher tumor-to-parenchyma CNR than pooled C/D categories in both modalities (PC-CT: 6.0 ± 3.5 (95%-CI [3.9; 8.1]) vs. 5.5 ± 3.7 (95%-CI [3.6; 7.3]), p = 0.687; MRI: 7.0 ± 4.0 (95%-CI [4.6; 9.4]) vs. 6.5 ± 4.4 (95%-CI [4.3; 8.7]), p = 0.748). Tumor-to-parenchyma CNR stratified by breast density is provided in Supplemental Table 1.

Tumor diameters

In the 31 paired axial target lesion measurements, largest axial tumor diameter were slightly larger in MRI than PC-CT (31.3 ± 21.4 mm versus 29.5 ± 21.2 mm; mean paired difference 1.7 mm, 95% CI 0.6–2.9 mm; paired t-test, $p = 0.005$). Median largest diameter was 26.0 mm [IQR 17.5–35.0] on MRI and 24.0 mm [IQR 16.0–32.5] on PC-CT. Short-axis diameters were comparable ($p = 0.420$). The axial area product was larger on MRI by Wilcoxon signed-rank testing (median paired difference 50.0 mm² [IQR 4.5–104.0]; $p = 0.007$), although the mean paired difference was small and its 95% CI crossed zero (16.1 mm², 95% CI: -73.9–106.0 mm²). Detailed descriptive statistics are provided in Supplemental Table 2 and 3. Using the predefined long-axis size categories, PC-CT and MRI were concordant in 26/31 target lesions (84%). Five of 31 target lesions (16%) shifted by one

adjacent long-axis size category between modalities. MRI assigned a larger category in four cases and a smaller category in one case. Without an untreated whole-specimen pathology reference, these findings indicate intermodality disagreement but do not establish overestimation or underestimation by either technique. In the five discordant cases, the category shift was limited to one adjacent size category; MRI assigned a larger size category in four cases and a smaller size category in one case (Table 3).

T-stages

Imaging-based T categories assigned on PC-CT and MRI were identical for both readers (Table 2). This represents descriptive intermodality concordance and not pathology-referenced staging accuracy. No inferential comparison between imaging-based T-category and pathological T category was performed, because 24/32 patients had received neoadjuvant systemic therapy before surgery and ypT therefore did not provide a uniform untreated reference standard.

BPE analysis

Median BPE intensity was significantly lower in PC-CT than in MRI (R1: 1 [IQR 1–2], R2: 1 [IQR 1–2] vs. R1: 2 [1–3], R2: 2 [2–3]; $p < 0.001$), for more detailed data see Figure 3 and 4, Table 4 and 5. Breast density did not influence BPE intensity significantly (PC-CT_{C+}: $p = 0.586$, PC-CT_{Iodine}: $p = 0.442$, MRI: $p = 0.481$). In an exploratory analysis including 14 premenopausal and 16 postmenopausal women, median BPE ratings were lower on PC-CT than on MRI in both pre- and postmenopausal women for both readers. Detailed descriptive results are provided in Supplemental Table 4. No interference regarding a modality-by-menopausal status was made. Overall interreader agreement for BPE intensity was moderate for PC-CT monoenergetic post-contrast images (linear-weighted $\kappa = 0.513$) and substantial for PC-CT iodine maps ($\kappa = 0.669$) and MRI ($\kappa = 0.773$). Category-specific agreement and Holm-adjusted p values are reported in Table 5. Minimal BPE was assigned more frequently on PC-CT iodine maps than on MRI by both readers (both $p < 0.001$). The remaining adjusted p values ranged from 0.067 to 1.000 and are reported individually in Table 5. Both readers selected iodine maps as the preferred PC-CT reconstruction for depicting BPE in 32/32 cases.

306 **DCIS suspicion and interreader agreement**

307 Both readers identified the single pure DCIS case. Among 7 cancers with pathology reported associated DCIS,
308 each reader suspected an associated in situ component in three cases and missed four. Reader 1 additionally
309 suspected associated DCIS in seven cases without pathology-reported associated DCIS, whereas reader 2 did so
310 in five cases. The high interreader agreement was almost perfect ($\kappa = 0.851$), however, pathology-referenced
311 counts demonstrated both overcalling and undercalling. It reflects reproducibility between readers and should not
312 be interpreted as evidence of diagnostic accuracy.

313 **Discussion**

314 In this retrospective intra-individual comparison, thoracoabdominal PC-CT using a free-hanging breast protocol
315 demonstrated significantly lower BPE than breast MRI whereas lesion CNR did not differ significantly between
316 modalities, although MRI tended to show higher tumor-to-parenchyma CNR, whereas PC-CT showed higher
317 tumor-to-fat CNR. Tumor-to-parenchyma CNR was higher in the lower breast density categories, without
318 reaching statistical significance. MRI yielded slightly larger long-axis measurements, and 5/31 target lesions
319 shifted by one adjacent size category. Imaging-based T-category concordance and DCIS observations were
320 secondary descriptive findings and should not be interpreted as evidence of staging accuracy or diagnostic
321 performance. The lower BPE may be advantageous when lesion assessment on MRI is limited by moderate or
322 marked BPE.
323
324 The observed findings reflect fundamental differences in image formation and contrast mechanisms between the
325 two modalities. PC-CT relies on iodinated contrast agents, with X-ray attenuation increasing approximately
326 linearly with iodine concentration, thereby predominantly reflecting vascularity (38). Iodine maps are therefore
327 well suited for objective, quantitative BPE evaluation. Despite improved spatial resolution, PC-CT remains
328 constrained by lower intrinsic soft-tissue contrast and higher image noise (35). In contrast, MRI benefits from
329 intrinsically high soft-tissue contrast, efficient fat suppression and larger voxel size, resulting in higher CNR. The
330 non-linear T1-signal response of gadolinium amplifies contrast differences even with small variations in
331 gadolinium concentration (39). As a result, hormonally driven microvascular changes may be accentuated on
332 MRI but remain below the detection threshold of CT-based modalities, contributing to the consistently lower
333 BPE observed on PC-CT and may also explain why MRI tends to measure larger tumor diameters than CT. MRI

is known to slightly overestimate pathologic tumor sizes (40, 41), likely due to reactive peritumoral changes or tissue shrinkage after fixation (42-44). PC-CT is expected to depict fewer reactive changes compared to MRI, contributing to smaller measured tumor extents and lower apparent BPE. Importantly, the observed differences did not affect clinical T-stage categorization in our cohort. Although the mean long-axis difference was modest, 5/31 target lesions crossed one adjacent size-category threshold. The identical imaging-based T-category assignments therefore do not eliminate potentially relevant continuous size disagreement, particularly for lesions close to clinical size thresholds. This is in line with a recent prospective study showing concordance of tumor sizes, T-category and tumor morphology between MRI and PC-CT and histologic specimen sizes (45).

Moderate or marked BPE is considered a major limitation of breast MRI, as it increases false-positive interpretations (18, 46), leads to additional imaging and biopsies (18, 20), and reduces diagnostic accuracy (21). Stronger BPE decreases MRI's sensitivity (95% to 84%) and specificity (89% to 75-79%) (22, 31). Similar observations have been reported for CESM, with reduced sensitivity (79% vs. 91%) and specificity (76% vs. 92%) (47). While BPE has been extensively characterized in MRI and CESM (2, 3, 12), its appearance and clinical relevance in CT-based breast imaging remains mostly unexplored. To date, only one study has evaluated BPE using a CT-based technique. Ma et al. (2022) reported substantial agreement between CE CB-BCT and breast MRI for qualitative BPE assessment in their comparative study. Consistent with our findings, CE CB-BCT yielded generally lower BPE level (32). However, their acquisition protocol differed substantially from ours (49 kVp, 50-80 mAs, 90 mL Iohexol, 300 mg I/mL @2.0-2.5 mL/s). A fundamental limitation of the dedicated breast CT setup is the single breast imaging at a given time point, which restricts simultaneous assessment of both breasts (48). This contributed to the prolonged acquisition times in their study (120 seconds and 180 seconds contralateral) (32).

In the present study, BPE was consistently lower on PC-CT_{C+} and PC-CT_{Iodine} compared with MRI, when using identical BPE descriptors. Menopausal status and tumor subtype distribution aligned with established epidemiology (49, 50), and premenopausal women demonstrated higher BPE level in both modalities, consistent with prior MRI- and CESM studies (3, 12). Although our cohort included a higher proportion of dense breasts (51, 52), likely reflecting a high-risk referral pattern, breast density was not associated with BPE in either modality, in agreement with prior reports (6, 25).

Acquisition timing may also have influenced the appearance of BPE. A key strength of our study is the same-day MRI and PC-CT examinations with almost identical acquisition times (80-90 seconds post-injection). In MRI, early acquisition (60-80 seconds) during the peak enhancement phase (~90 seconds), performed before plateau phase (210-320 seconds), maximizes lesion-to-parenchyma contrast (1, 53). Assuming a well-chosen timing in the late arterial or early portal venous phase, which typically yields high contrast, the lower BPE in PC-CT is unlikely to be attributable to temporal differences and instead reflects modality-specific contrast kinetics and signal characteristics.

Reduced parenchymal masking in PC-CT has several potential clinical implications. Image interpretation may be facilitated in patients with pronounced BPE on MRI, particularly for small or moderately enhancing lesions that may otherwise be obscured. Non-mass enhancing lesions, including DCIS, are especially challenging in the presence of strong BPE (8, 23). CT-based breast imaging appears to share diagnostic characteristics with MRI in this regard. Kang et al. (2021) reported a high positive predictive value of approximately 94-95% for detecting malignant non-mass enhancement in CE CB-BCT (54). Consistent with this, we observed substantial to near-perfect interreader agreement for DCIS suspicion with PC-CT, aligning with recent evidence of high sensitivity (88%) and specificity (99%) for detection of DCIS adjacent to breast cancer using prone, CE PC-CT in a staging setting (55). In the present cohort, however, the grading for associated DCIS was incomplete with missing grading status in 3/7 cases. Lower apparent BPE on PC-CT did not translate into reliable pathology-referenced depiction of associated DCIS. Moreover, the high interreader agreement should not be interpreted as evidence of diagnostic accuracy, rather, it reflects the reproducibility of identifying imaging findings attributed to associated DCIS on PC-CT.

Nevertheless, readers' confidence in evaluating CT for breast imaging may currently be limited by sparse evidence, lack of experience and missing diagnostic criteria. Direct application of MRI-based BI-RADS BPE categories to CT may be inappropriate, as BPE might not have the same clinical implications across modalities (36). The absence of concordant moderate or marked PC-CT iodine-map ratings further underscores the exploratory, non-validated nature of the adapted PC-CT BPE intensity score and the need for validation in larger cohorts. Instead, alternative classification strategies emphasizing lesion conspicuity relative to BPE, similar to

approaches shown to improve specificity in CESM, may be more suitable (56). As lesion conspicuity in CE PC-CT appears largely independent of BPE strength and breast density (35, 57), we assume–that parenchymal masking is less clinically relevant for CT, supported by unchanged clinical imaging-based T-stage assessments. However, reporting BPE may nevertheless be useful in selected scenarios, such as when asymmetry or non-mass enhancement complicates interpretation or when cross-modality comparisons with MRI need to be addressed.

Quantitative imaging biomarkers for risk prediction are increasingly important in personalized medicine. Moderate to marked BPE on MRI has been identified as an independent risk factor for increased breast cancer risk, irrespective of menopausal status (58), with reported odds ratios ranging from approximately 2-3 (1, 9, 25, 28, 59) and up to 9-10 for MRI (25, 30), and an odds ratio of 2.2 for strong BPE in CESM (28). Moreover, reductions in BPE during neoadjuvant chemotherapy correlate with pathological complete response (19, 24) and, to a lesser extent, in CB-BCT (60). MRI-based BPE assessment remains subjective and variable due to heterogeneous signal characteristics (61, 62). In contrast, PC-CT enables objective iodine quantification of BPE and breast density, allowing reproducible and potentially automated BPE measurements, analogous to texture-based approaches used for breast density (63). This may reduce observer variability, improve standardized reporting, and facilitate integration into risk stratification models and artificial-intelligence-based workflows, which may further improve individualized risk assessment. Despite these promising developments, the role of PC-CT as an imaging biomarker for breast cancer risk assessment and treatment response has yet to be established.

Several limitations should be acknowledged. First, the retrospective design limited the availability of clinical history, including hormone therapy, contraceptive use, menstrual cycle phase, and serum hormone levels, precluding systematic assessment of endocrine effects on background parenchymal enhancement (BPE). Two patients were receiving tamoxifen, which may reduce BPE and may therefore have biased the comparison toward lower enhancement in this small cohort [14, 16]. Second, the cohort was small because inclusion required same-day photon-counting CT (PC-CT) and breast MRI, and all patients had biopsy-proven breast cancer, limiting generalizability to screening or non-cancer populations. Manual single-reader ROI placement and variable ROI size introduced operator dependence. Although predefined avoidance criteria and anatomical matching were applied, selection of the most enhancing viable tumor component may have affected CNR estimates, and measurement reproducibility was not assessed. Third, associated DCIS extent was not measured separately, and pretreatment core-biopsy reports did not consistently provide a separate nuclear grade for the associated in situ

component in 3 cases. This precluded grade-stratified analysis of DCIS enhancement and restricts all DCIS-related observations to descriptive, hypothesis-generating findings. This limitation does not affect the primary intraindividual comparison of BPE. Fourth, pathology-based T-stage accuracy could not be assessed: only 8/32 patients underwent upfront surgery, whereas most surgical T categories represented post-neoadjuvant residual disease rather than untreated tumor extent at baseline imaging. Accordingly, T-category analysis was restricted to PC-CT–MRI concordance and should be interpreted as an inter-modality comparison rather than an accuracy analysis. Finally, radiation exposure precludes routine multiphase PC-CT acquisitions, limiting assessment of optimal contrast timing and dynamic cross-modality comparisons.

Future studies with larger, prospective, vendor-comparative cohorts are needed to establish clinically relevant descriptors for multi-energy CT, optimize contrast timing, and determine whether the reduced BPE with preserved lesion contrast improves diagnostic performance. Spectral dual-energy CT and PC-CT may enable quantitative iodine-based assessment of BPE and density, although their value for risk prediction or treatment-response assessment remains unproven. In this small retrospective cancer-only cohort, prone photon-counting CT showed lower apparent BPE than same-day breast MRI. These differences likely reflect modality-specific contrast mechanisms and acquisition physics rather than true variations in parenchymal vascularity. No significant intermodal difference in lesion CNR was detected, whereas MRI yielded a mean 1.7-mm larger long-axis measurement and five target lesions crossed one adjacent size category. Without an untreated pathology reference, these findings establish intermodal differences but not greater accuracy or clinical utility of either modality.

Conclusions

Lower apparent background parenchymal enhancement (BPE) on PC-CT may reduce parenchymal masking. However, size differences and absent pathology correlation require prospective validation before clinical implications can be established. These findings support PC-CT as a potential complementary diagnostic option when MRI is unavailable, contraindicated or limited by marked BPE, but they do not establish diagnostic performance, DCIS suspicion, or clinical benefit.

Abbreviations

BI-RADS	Breast Imaging Reporting and Data System
BPE	Background parenchymal enhancement
CB-BCT	Cone-beam breast CT
CE	Contrast enhanced
CESM	Contrast-enhanced spectral mammography
CNR	Contrast-to-noise ratio
$CTDI_{vol}$	CT Dose volume index
DCIS	Ductal carcinoma in situ
DLP	Dose-length product
ER	Estrogen receptor
IHC	Immunohistochemistry
ISH	In situ hybridization
IQR	Interquartile range
HER2	Human epidermal growth factor receptor 2
MRI	Magnetic resonance imaging
PC-CT	Photon-counting CT
$PC\text{-}CT_{Iodine}$	Photon-counting CT iodine-map reconstruction
$PC\text{-}CT_{C+}$	65-keV monoenergetic post-contrast photon-counting CT reconstruction
PR	Progesterone receptor
ROI	Region of interest
SD	Standard deviation

References

1. Liao GJ, Henze Bancroft LC, Strigel RM, Chitalia RD, Kontos D, Moy L, et al. Background parenchymal enhancement on breast MRI: a comprehensive review. Journal of Magnetic Resonance Imaging. 2020;51(1):43-61.

2. Sogani J, Morris EA, Kaplan JB, D'Alessio D, Goldman D, Moskowitz CS, et al. Comparison of background parenchymal enhancement at contrast-enhanced spectral mammography and breast MR imaging. Radiology. 2017;282(1):63-73.

3. Karimi Z, Phillips J, Slanetz P, Lotfi P, Dialani V, Karimova J, et al. Factors associated with background parenchymal enhancement on contrast-enhanced mammography. American journal of roentgenology. 2021;216(2):340-8.

4. King V, Gu Y, Kaplan JB, Brooks JD, Pike MC, Morris EA. Impact of menopausal status on background parenchymal enhancement and fibroglandular tissue on breast MRI. European radiology. 2012;22(12):2641-7.

5. Sung JS, Corben AD, Brooks JD, Edelweiss M, Keating DM, Lin C, et al. Histopathologic characteristics of background parenchymal enhancement (BPE) on breast MRI. Breast cancer research and treatment. 2018;172(2):487-96.

6. Hansen NL, Kuhl CK, Barabasch A, Strobel K, Schrading S. Does MRI breast "density"(degree of background enhancement) correlate with mammographic breast density? Journal of Magnetic Resonance Imaging. 2014;40(2):483-9.

7. Brooks JD, Sung JS, Pike MC, Orlow I, Stanczyk FZ, Bernstein JL, et al. MRI background parenchymal enhancement, breast density and serum hormones in postmenopausal women. Int J Cancer. 2018;143(4):823-30.

8. Giess CS, Yeh ED, Raza S, Birdwell RL. Background parenchymal enhancement at breast MR imaging: normal patterns, diagnostic challenges, and potential for false-positive and false-negative interpretation. Radiographics. 2014;34(1):234-47.

9. Kajihara M, Goto M, Hirayama Y, Okunishi S, Kaoku S, Konishi E, et al. Effect of the menstrual cycle on background parenchymal enhancement in breast MR imaging. Magnetic resonance in medical sciences. 2013;12(1):39-45.

10. Kuhl CK, Bieling HB, Gieseke J, Kreft BP, Sommer T, Lutterbey G, et al. Healthy premenopausal breast parenchyma in dynamic contrast-enhanced MR imaging of the breast: normal contrast medium enhancement and cyclical-phase dependency. Radiology. 1997;203(1):137-44.

11. Müller-Schimpfle M, Ohmenhaüser K, Stoll P, Dietz K, Claussen CD. Menstrual cycle and age: influence on parenchymal contrast medium enhancement in MR imaging of the breast. Radiology. 1997;203(1):145-9.

12. Nissan N, Anaby D, Mahameed G, Bauer E, Moss Massasa EE, Menes T, et al. Ultrafast DCE-MRI for discriminating pregnancy-associated breast cancer lesions from lactation related background parenchymal enhancement. European Radiology. 2023;33(11):8122-31.

13. Huck LC, Truhn D, Wilpert C, Zanderigo E, Raaff V, Dethlefsen E, et al. Background parenchymal enhancement in contrast-enhanced MR imaging suggests systemic effects of intrauterine contraceptive devices. European Radiology. 2022;32(11):7430-8.

14. King V, Kaplan J, Pike MC, Liberman L, David Dershaw D, Lee CH, et al. Impact of tamoxifen on amount of fibroglandular tissue, background parenchymal enhancement, and cysts on breast magnetic resonance imaging. The breast journal. 2012;18(6):527-34.

15. Heller SL, Young Lin LL, Melsaether AN, Moy L, Gao Y. Hormonal effects on breast density, fibroglandular tissue, and background parenchymal enhancement. Radiographics. 2018;38(4):983-96.

16. Schrading S, Schild H, Kühr M, Kuhl C. Effects of tamoxifen and aromatase inhibitors on breast tissue enhancement in dynamic contrast–Enhanced breast MR imaging: a longitudinal intraindividual cohort study. Radiology. 2014;271(1):45-55.

17. Preibsch H, Wanner L, Bahrs S, Wietek B, Siegmann-Luz K, Oberlecher E, et al. Background parenchymal enhancement in breast MRI before and after neoadjuvant chemotherapy: correlation with tumour response. European radiology. 2016;26(6):1590-6.

18. DeMartini WB, Liu F, Peacock S, Eby PR, Gutierrez RL, Lehman CD. Background parenchymal enhancement on breast MRI: impact on diagnostic performance. American Journal of Roentgenology. 2012;198(4):W373-W80.

19. Rella R, Contegiacomo A, Bufi E, Mercogliano S, Belli P, Manfredi R. Background parenchymal enhancement and breast cancer: a review of the emerging evidences about its potential use as imaging biomarker. The British Journal of Radiology. 2021;94(1119):20200630.

20. Hambly NM, Liberman L, Dershaw DD, Brennan S, Morris EA. Background parenchymal enhancement on baseline screening breast MRI: impact on biopsy rate and short-interval follow-up. American Journal of Roentgenology. 2011;196(1):218-24.

21. Telegrafo M, Rella L, Ianora AS, Angelelli G, Moschetta M. Effect of background parenchymal enhancement on breast cancer detection with magnetic resonance imaging. Diagnostic and Interventional Imaging. 2016;97(3):315-20.

22. Bechyna S, Baltzer PA. Impact of background parenchymal enhancement on diagnostic performance of breast MRI: a systematic review and meta-analysis. Radiology. 2025;315(2):e241919.

23. Park S, Kang D, Kim T. Does background parenchymal enhancement on MRI affect the rate of positive resection margin in breast cancer patients? The British Journal of Radiology. 2015;88(1046):20140638.

24. Bauer E, Levy MS, Domachevsky L, Anaby D, Nissan N. Background parenchymal enhancement and uptake as breast cancer imaging biomarkers: a state-of-the-art review. Clinical Imaging. 2022;83:41-50.

25. King V, Brooks JD, Bernstein JL, Reiner AS, Pike MC, Morris EA. Background parenchymal enhancement at breast MR imaging and breast cancer risk. Radiology. 2011;260(1):50-60.

26. Thompson CM, Mallawaarachchi I, Dwivedi DK, Ayyappan AP, Shokar NK, Lakshmanaswamy R, et al. The association of background parenchymal enhancement at breast MRI with breast cancer: a systematic review and meta-analysis. Radiology. 2019;292(3):552-61.

27. Hu N, Zhao J, Li Y, Fu Q, Zhao L, Chen H, et al. Breast cancer and background parenchymal enhancement at breast magnetic resonance imaging: a meta-analysis. BMC Medical Imaging. 2021;21(1):32.

28. Sorin V, Yagil Y, Shalmon A, Gotlieb M, Faermann R, Halshtok-Neiman O, et al. Background parenchymal enhancement at contrast-enhanced spectral mammography (CESM) as a breast cancer risk factor. Academic radiology. 2020;27(9):1234-40.

29. Sippo DA, Rutledge GM, Burk KS, Mercaldo SF, Dontchos BN, Edmonds CE, et al. Effect of background parenchymal enhancement on cancer risk across different high-risk patient populations undergoing screening breast MRI. American Journal of Roentgenology. 2019;212(6):1412-8.

30. Dontchos BN, Rahbar H, Partridge SC, Korde LA, Lam DL, Scheel JR, et al. Are qualitative assessments of background parenchymal enhancement, amount of fibroglandular tissue on MR images, and mammographic density associated with breast cancer risk? Radiology. 2015;276(2):371-80.

31. Ray KM, Kerlikowske K, Lobach IV, Hofmann MB, Greenwood HI, Arasu VA, et al. Effect of Background Parenchymal Enhancement on Breast MR Imaging Interpretive Performance in Community-based Practices. Radiology. 2018;286(3):822-9.

32. Ma Y, Liu A, Zhang Y, Zhu Y, Wang Y, Zhao M, et al. Comparison of background parenchymal enhancement (BPE) on contrast-enhanced cone-beam breast CT (CE-CBBCT) and breast MRI. European Radiology. 2022;32(8):5773-82.

33. Willemink MJ, Persson M, Pourmorteza A, Pelc NJ, Fleischmann D. Photon-counting CT: technical principles and clinical prospects. Radiology. 2018;289(2):293-312.

34. Varga-Szemes A, Emrich T. Photon-counting detector CT: a disrupting innovation in medical imaging. European Radiology Experimental. 2025;9(1):38.

35. Wilpert C, Pichotka MP, Molina-Fuentes MF, Weiss J, Bamberg F, Windfuhr-Blum M, et al. Prone Photon-counting Computed Tomography With Iodine Mapping for Differentiating Breast Masses: A Prospective Study. Invest Radiol. 2026;61(9):595-604.

36. Newell D, Leung JWT, DeMartini WB, Lee CH, Eby PR. ACR BI-RADS v2025 Manual. Reston, VA: American College of Radiology; 2025.

37. Landis JR, Koch GG. The measurement of observer agreement for categorical data. Biometrics. 1977;33(1):159-74.

38. Donabauer M, Sawall S, Ayx I, Wangler C, Schoenberg SO, Wangler B. Development and characterization of new contrast agents for Photon-Counting CT. Eur J Radiol. 2025;195:112643.

39. Kanal E, Maki JH, Schramm P, Marti-Bonmati L. Evolving Characteristics of Gadolinium-Based Contrast Agents for MR Imaging: A Systematic Review of the Importance of Relaxivity. J Magn Reson Imaging. 2025;61(1):52-69.

40. Marinovich ML, Macaskill P, Irwig L, Sardanelli F, Mamounas E, von Minckwitz G, et al. Agreement between MRI and pathologic breast tumor size after neoadjuvant chemotherapy, and comparison with alternative tests: individual patient data meta-analysis. BMC Cancer. 2015;15:662.

41. Pop CF, Stanciu-Pop C, Drisis S, Radermeker M, Vandemerckt C, Noterman D, et al. The impact of breast MRI workup on tumor size assessment and surgical planning in patients with early breast cancer. Breast J. 2018;24(6):927-33.

42. Pritt B, Tessitore JJ, Weaver DL, Blaszyk H. The effect of tissue fixation and processing on breast cancer size. Hum Pathol. 2005;36(7):756-60.

43. Zaidi M, Khan S, Farooqi NB, Abbas K, Idrees R. Effect of formalin fixation on surgical margins in breast cancer surgical specimen. Int J Breast Cancer. 2014;2014:121838.

44. Horn CL, Naugler C. Breast specimen shrinkage following formalin fixation. Pathology and Laboratory Medicine International. 2014:11-4.

45. Fu Q, Zeng Y, Chang R, Xu Z, Zhan Y, Tan L, et al. Performance of Photon-counting CT for Assessing Pretreatment Breast Cancer: Comparison with Mammography, MRI, and (18)F-FDG PET/CT. Radiology. 2026;320(3):e253531.

46. Kim S-Y, Lee HS, Kim E-K, Kim MJ, Moon HJ, Yoon JH. Effect of background parenchymal enhancement on pre-operative breast magnetic resonance imaging: how it affects interpretation and the role of second-look ultrasound in patient management. Ultrasound in Medicine & Biology. 2016;42(12):2766-74.

47. Yuen S, Monzawa S, Gose A, Yanai S, Yata Y, Matsumoto H, et al. Impact of background parenchymal enhancement levels on the diagnosis of contrast-enhanced digital mammography in evaluations of breast cancer: comparison with contrast-enhanced breast MRI. Breast Cancer. 2022;29(4):677-87.

48. Zhu Y, O'Connell AM, Ma Y, Liu A, Li H, Zhang Y, et al. Dedicated breast CT: state of the art-Part II. Clinical application and future outlook. Eur Radiol. 2022;32(4):2286-300.

49. Leventea E, Harkness EF, Brentnall AR, Howell A, Evans DG, Harvie M. Is breast cancer risk associated with menopausal hormone therapy modified by current or early adulthood BMI or age of first pregnancy? Cancers. 2021;13(11):2710.

50. Renehan AG, Pegington M, Harvie MN, Sperrin M, Astley SM, Brentnall AR, et al. Young adulthood body mass index, adult weight gain and breast cancer risk: the PROCAS Study (United Kingdom). British journal of cancer. 2020;122(10):1552-61.

51. van der Waal D, den Heeten GJ, Pijnappel RM, Schuur KH, Timmers JM, Verbeek AL, et al. Comparing visually assessed BI-RADS breast density and automated volumetric breast density software: a cross-sectional study in a breast cancer screening setting. PLoS One. 2015;10(9):e0136667.

52. Sickles EA. ACR BI-RADS® Atlas, Breast imaging reporting and data system. American College of Radiology. 2013:39.

53. Melsaether A, Pujara AC, Elias K, Pysarenko K, Gudi A, Dodelzon K, et al. Background parenchymal enhancement over exam time in patients with and without breast cancer. J Magn Reson Imaging. 2017;45(1):74-83.

54. Kang W, Zhong W, Su D. The cone-beam breast computed tomography characteristics of breast non-mass enhancement lesions. Acta Radiologica. 2021;62(10):1298-308.

55. Neubauer J, Wilpert C, Gebler O, Taran F-A, Pichotka M, Stein T, et al. Diagnostic accuracy of contrast-enhanced thoracic photon-counting computed tomography for opportunistic locoregional staging of breast cancer compared with digital mammography: a prospective trial. Investigative Radiology. 2024;59(7):489-94.

56. Allajbeu I, Nanaa M, Manavaki R, Papalouka V, Bene I, Payne N, et al. Improving the diagnostic performance of contrast-enhanced mammography through lesion conspicuity and enhancement quantification. European Radiology. 2025:1-13.

57. Wetzl M, Heilingbrunner T, Heindl F, Wenkel E, Uder M, Ohlmeyer S. Detectability of Breast Cancer in Dedicated Breast CT Compared With Mammography Dependent on Breast Density. Invest Radiol. 2024;59(12):861-5.

58. Telegrafo M, Rella L, Ianora AAS, Angelelli G, Moschetta M. Breast MRI background parenchymal enhancement (BPE) correlates with the risk of breast cancer. Magnetic resonance imaging. 2016;34(2):173-6.

59. Niell BL, Abdalah M, Stringfield O, Raghunand N, Ataya D, Gillies R, et al. Quantitative Measures of Background Parenchymal Enhancement Predict Breast Cancer Risk. AJR Am J Roentgenol. 2021;217(1):64-75.

60. Wang Y, Ma Y, Liu A, Zhao M, Zhu Y, Yin L, et al. Longitudinal contrast-enhanced cone beam breast computed tomography for monitoring treatment response in breast cancer neoadjuvant therapy: a comprehensive assessment. Breast Cancer Research. 2025;27(1):199.

61. Pujara AC, Mikheev A, Rusinek H, Gao Y, Chhor C, Pysarenko K, et al. Comparison between qualitative and quantitative assessment of background parenchymal enhancement on breast MRI. J Magn Reson Imaging. 2018;47(6):1685-91.

62. Muller-Franzes G, Khader F, Tayebi Arasteh S, Huck L, Bode M, Han T, et al. Intraindividual Comparison of Different Methods for Automated BPE Assessment at Breast MRI: A Call for Standardization. Radiology. 2024;312(1):e232304.

63. Landsmann A, Ruppert C, Wieler J, Hejduk P, Ciritsis A, Borkowski K, et al. Radiomics in photon-counting dedicated breast CT: potential of texture analysis for breast density classification. Eur Radiol Exp. 2022;6(1):30.

Tables

Table 1. Patient characteristics

	Value
Age, years, mean ± standard deviation	53 ± 14
Sex (n=32)	
Female	31 (97%)
Male	1 (3%)
Menopausal status (women only, n= 31)	
Premenopausal	14 (45%)
Perimenopausal	1 (3%)
Postmenopausal	16 (52%)
Endocrine therapy at the time of imaging (n = 32)	
No endocrine therapy	30 (94%)
Tamoxifen	2 (6%)
Parity, women only (n = 31)	
0 births	8 (26%)
1 birth	16 (52%)
2 births	4 (13%)
3 births	2 (6%)
4 births	1 (3%)
Mammographic breast density (n = 32)	
A (almost entirely fat)	3 (9%)
B (fibroglandular tissue)	10 (31%)
C (heterogeneously dense)	8 (25%)
D (extremely dense)	11 (34%)

Values are presented as n (%) unless otherwise indicated. Percentages were calculated using the denominator specified for each section and may not sum to 100% because of rounding. Menopausal status and parity are reported for women only; these variables were not applicable to the male participant.

BI-RADS (Breast Imaging Reporting and Data System); Density categories: A = almost entirely fatty, B = scattered fibroglandular density, C = heterogeneously dense, D = extremely dense.

657 **Table 2.** Tumor characteristics and biomarker status

Histologic finding, all index tumors (n = 32)	***n***	***%***
Invasive cancers of no special type	22	69%
Invasive cancers of no special type with associated DCIS	7	22%
Invasive lobular carcinomas	2	6%
Pure DCIS	1	3%
Histological grade, invasive index tumors (n = 31)		
G1	0	0%
G2	22	71%
G3	9	29%
Nuclear grade of associated DCIS (n = 7)		
Low grade	1	14%
Intermediate grade	1	14%
High grade	2	29%
Not separately reported	3	43%
Estrogen receptor status, invasive index tumors (n = 31)		
Negative (<1% nuclear staining)	8	26%
Positive (≥1% nuclear staining)	23	74%
Progesterone receptor status, invasive index tumors (n = 31)		
Negative (<1% nuclear staining)	14	45%
Positive (≥1% nuclear staining)	17	55%
HER2 status, invasive index tumors (n = 31)		
HER2 positive	12	39%
HER2 negative, total	19	61%
Of these: IHC 0	9	29%
Of these: HER2 low	10	32%
Ki-67 proliferation index, invasive index tumors (n=31)		
< 20%	5	16%
≥20%	26	84%
Imaging-based clinical T-stage (PC-CT/MRI)		
1	7/7	22%
1a	2/2	6/6%
1b	1/1	3/3%
1c	4/4	13/13%
2	13/13	41/41%
3	4/4	13/13%
4	7/7	22/22%

Tis	1/1	3%
Clinical N category (n = 32)		
N0	20	63%
N1	12	38%
Clinical M category (n = 32)		
M0	30	94%
M1	2	6%
Surrogate subtype (n = 31)		
Luminal A-like	5	16%
Luminal B-like, HER2-negative	10	32%
Luminal B-like, HER2-positive	7	23%
HER2-enriched	5	16%
Triple-negative	4	13%

PC-CT/MRI denote the number of cases assigned to each T-category by each modality. Histological diagnoses are reported for all 32 index tumors. Histological grade and biomarker status are reported for the 31 invasive index tumors; the patient with pure DCIS is excluded from these analyses. ER, PR, HER2, and Ki-67 results refer to the same invasive index tumor in each patient. HER2-positive status was defined as IHC 3+ or IHC 2+ with positive ISH. HER2-negative tumors were subdivided descriptively into IHC 0 and HER2-low, defined as IHC 1+ or IHC 2+ with negative ISH. The IHC 0 and HER2-low rows are subdivisions of the HER2-negative total. All biomarker percentages use the denominator of 31 invasive index tumors and may not sum to 100% because of rounding.

DCIS = ductal carcinoma in situ; ER = estrogen receptor; HER2 = human epidermal growth factor receptor 2; IHC = immunohistochemistry; ISH = in situ hybridization; PR = progesterone receptor.

Table 3. Largest target lesion diameters on photon-counting CT (PC-CT) and MRI

Largest diameter (long axis category)	**PC-CT**	**MRI**
≤ 5 mm	1	1
6 - 10 mm	1	0
11 - 20 mm	9	9
21 - 50 mm	17	17
> 50 mm	3	4

Categories are based on the longest axial tumor diameters. Counts for each size category for PC-CT and MRI. Category disagreement between PC-CT and MRI occurred in 5/31 target lesions (16%), all shifts involved one adjacent size category.

MRI = magnetic resonance imaging, PC-CT = photon-counting CT

Table 4. Background parenchymal enhancement (BPE) in photon-counting CT (PC-CT) and MRI across readers.

	Reader 1	Reader 2		
BPE Intensity	**Median [IQR]**	**Median [IQR]**	**κ**	***p***
PC-CT$_{C+}$	1 [1-1]	1 [1-1]	0.513	
PC-CT$_{Iodine}$	1 [1-2]	1 [1-2]	0.669	reader 1 < 0.001, reader 2 < 0.001 (PC-CT vs. MRI)
MRI	2 [1-3]	2 [2-3]	0.773	

BPE = background parenchymal enhancement; IQR = interquartile range; κ = Cohen's kappa; MRI = magnetic resonance imaging; PC-CT = photon-counting CT; PC-CT$_{C+}$ = 65-keV monoenergetic post-contrast photon-counting CT reconstruction; PC-CT$_{Iodine}$ = Photon-counting CT iodine-map reconstruction.

Table 5. Reader-specific background parenchymal enhancement intensity ratings on PC-CT iodine maps and breast MRI.

Ordinal BPE category	PC-CT R1/R2, n	PC-CT category-specific agreement, %	MRI R1/R2, n	MRI category specific agreement, %	Holm-adjusted p, R1/R2
Minimal (1)	23/22	97.8	9/6	80.0	< 0.001/ < 0.001
Mild (2)	7/8	66.7	8/13	76.2	1.000/ 0.438
Moderate (3)	2/1	0.0	11/8	73.7	0.067/ 0.117
Marked (4)	0/1	0.0	4/5	66.7	0.250/ 0.438

Counts are shown as reader 1/reader 2 (R1/R2). Category-specific agreement denotes positive agreement for the respective category, calculated after dichotomization as that category versus all other categories. P values compare PC-CT iodine maps with MRI within each reader using exact McNemar tests and were Holm-adjusted across the four category-specific comparisons. Overall interreader agreement across the complete four-category ordinal scale was substantial for PC-CT iodine maps (linear-weighted $\kappa = 0.669$) and MRI ($\kappa = 0.773$).

BPE = background parenchymal enhancement, κ = Cohen's kappa, MRI = magnetic resonance imaging, PC-CT = Photon-counting CT; R1 = reader 1; R2 = reader 2

Figures

Figure 1. Flowchart of patient selection.

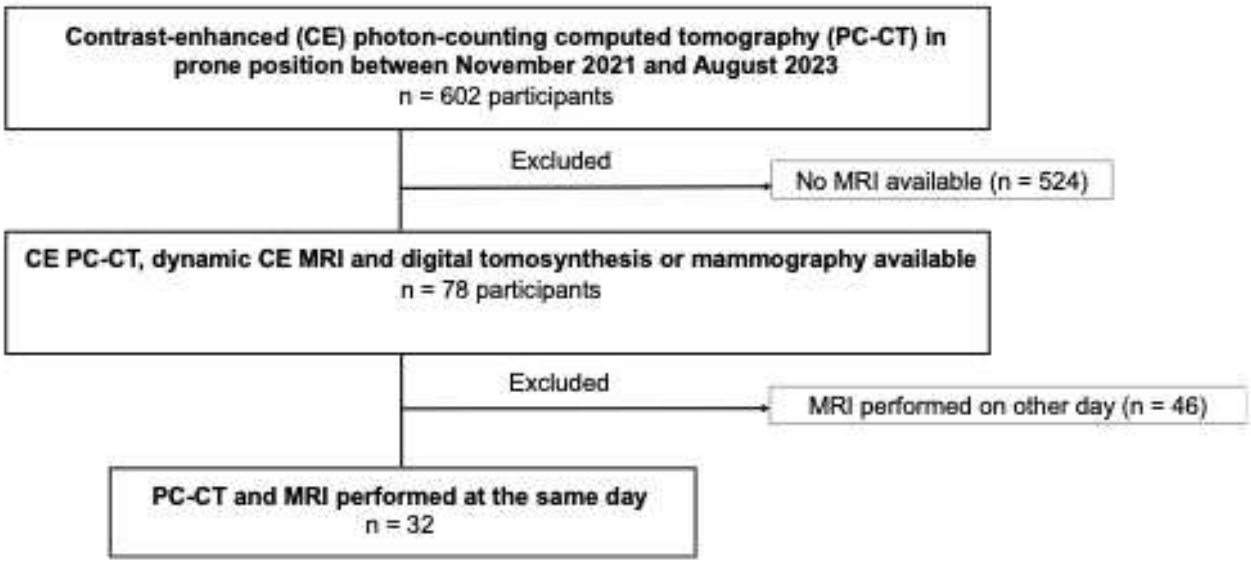
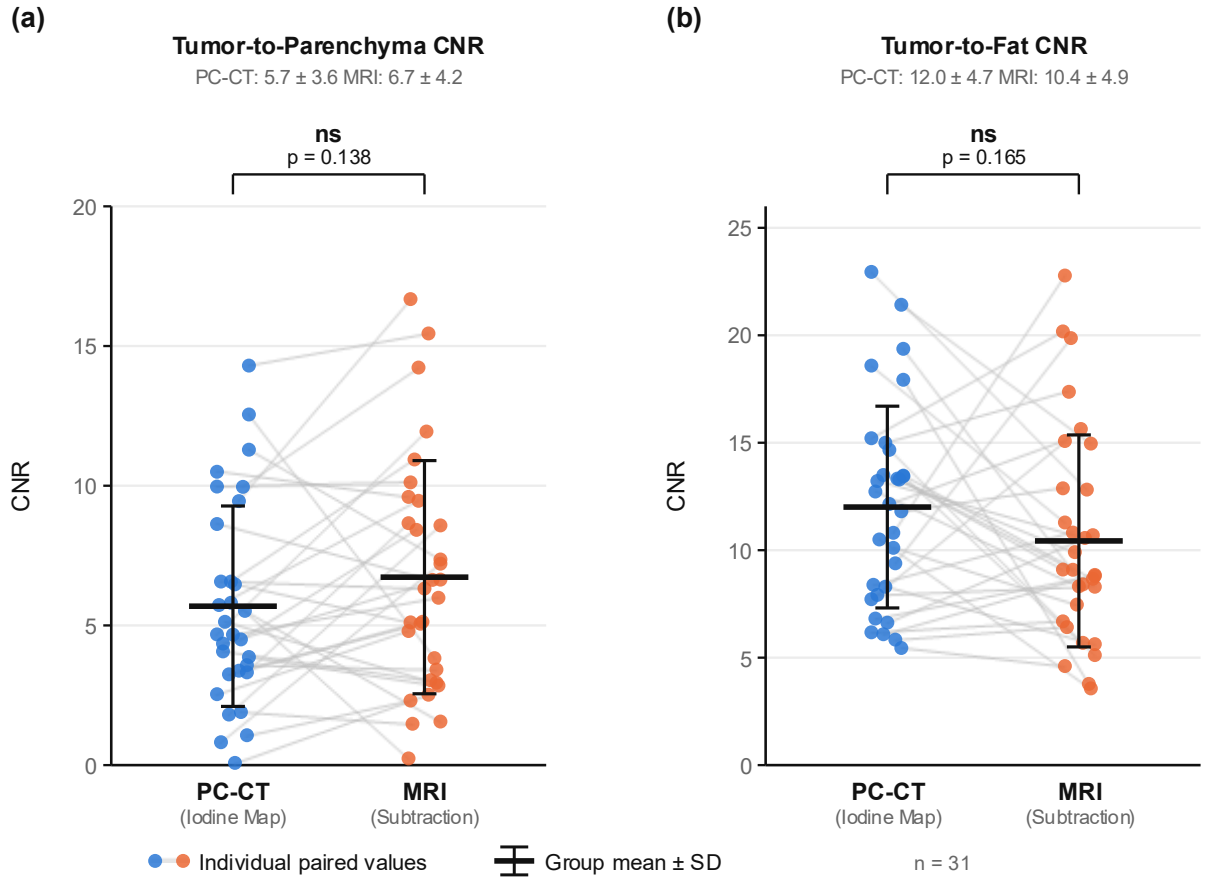


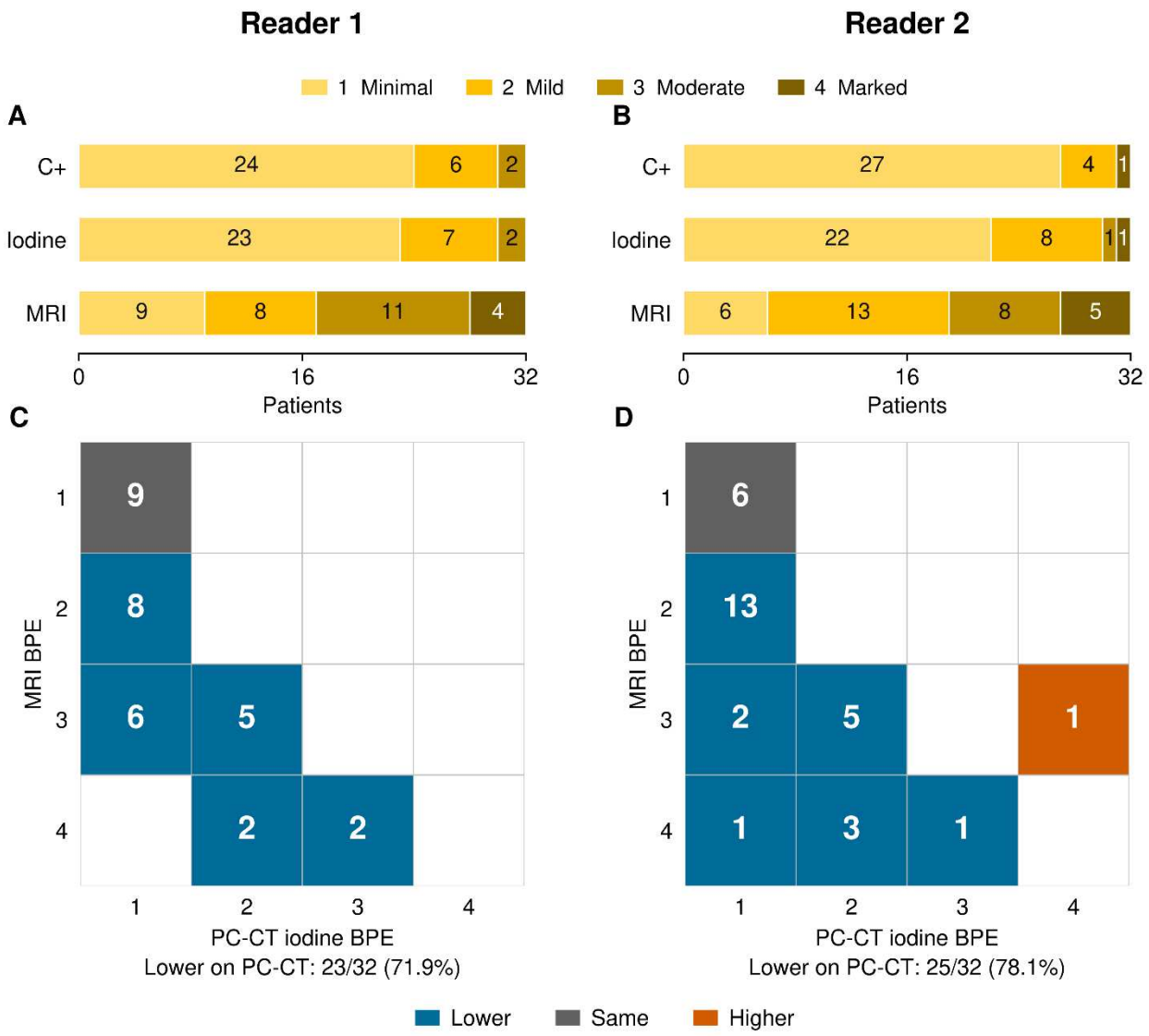
Figure 2. Contrast-to-noise ratios (CNR) of (a) tumor-to-parenchyma and (b) tumor-to-fat for photon-counting CT (PC-CT, Iodine Map) and MRI (subtraction imaging).



Each grey line connects the paired PC-CT and MRI values of a single patient. Dots represent individual measurements. The horizontal bar and vertical error bars indicate the group mean ± one standard deviation, respectively. Mean tumor-to-parenchyma CNR (a) was 5.7 ± 3.6 for PC-CT and 6.7 ± 4.2 for MRI; mean tumor-to-fat CNR (b) was 12.0 ± 4.7 for PC-CT and 10.4 ± 4.9 for MRI. Statistical comparisons are based on paired two-tailed t-tests (n = 31; the pure DCIS case was excluded from CNR analysis). P-values are shown above each bracket (ns $p \geq 0.05$).

CNR = contrast-to-noise ratio; DCIS = ductal carcinoma in situ; MRI = magnetic resonance imaging; PC-CT = photon-counting CT

Figure 3. Reader-specific distributions and paired comparisons of background parenchymal enhancement (BPE) on photon-counting CT (PC-CT) and MRI.

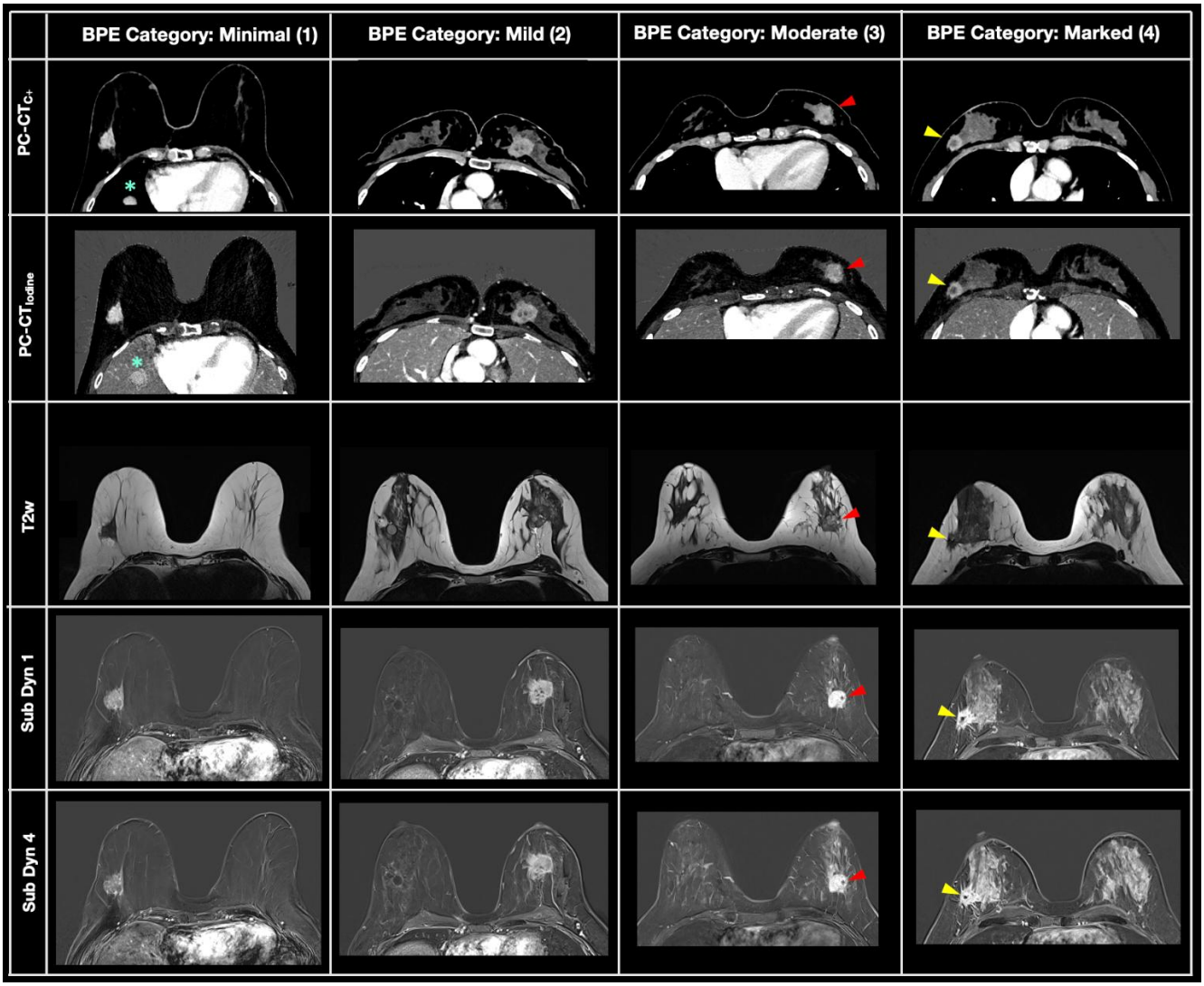


(A, B) Distribution of BPE ratings for readers 1 and 2 across 32 participants on 65-keV monoenergetic post-contrast PC-CT images (C+), PC-CT iodine maps (Iodine), and early post-contrast MRI subtraction images. Increasingly dark shades represent minimal (1), mild (2), moderate (3), and marked (4) BPE. Segment labels indicate participant counts. (C, D) Paired BPE ratings on MRI (rows) and PC-CT iodine maps (columns) for each reader. Numbers indicate participant counts; blank cells represent zero observations. Blue indicates lower BPE on PC-CT than on MRI, gray indicates the same category, and orange indicates higher BPE on PC-CT. Percentages below the matrices indicate the proportion of participants assigned a lower BPE category on PC-CT.

PC-CT ratings used a study-specific ordinal score adapted from the MRI BI-RADS BPE categories and do not represent a validated CT classification.

BPE = background parenchymal enhancement; MRI = magnetic resonance imaging; PC-CT = photon-counting CT.

Figure 4. Intraindividual comparison of background parenchymal enhancement (BPE) and tumor conspicuity in photon-counting CT (PC-CT) using a free-hanging breast protocol compared with breast MRI.



Columns are stratified by the MRI BPE category of the selected patients (minimal, mild, moderate, marked). Corresponding PC-CT images are displayed for intraindividual comparison and are not intended to represent validated PC-CT BPE categories. BPE was rated on a 4-point ordinal Likert scale adapted from the BI-RADS BPE Categories for MRI. Rows display corresponding PC-CT (upper) and MRI (lower). BPE appears consistently lower on PC-CT compared with MRI when compared intra-individually. The green star indicates a pulmonary metastasis in the right lung. The red arrowheads mark the breast cancer in the left breast and the yellow arrowheads the cancer in the right breast of another patient.

BPE = background parenchymal enhancement; MRI = magnetic resonance imaging; PC-CT = photon-counting CT; PC-CT_{C+} = 65-keV monoenergetic post-contrast photon-counting CT reconstruction; PC-CT_{Iodine} = Photon-counting CT iodine-map reconstruction.; Sub Dyn = Subtracted dynamic scan; T2w = T2 weighted

Supplement

Supplemental Tables

Supplemental Table 1. Tumor-to-Parenchyma contrast-to-noise ratio (CNR) for photon-counting CT (PC-CT) and MRI according to breast density.

Contrast-to-noise ratio (CNR) for three tissue pairs — tumor-to-parenchyma, tumor-to-fat, and parenchyma-to-fat — on photon-counting CT (PC-CT, Iodine Map) and MRI (subtraction imaging), stratified by mammographic breast density according to the ACR BI-RADS classification. Patients were pooled into a low-density group (BI-RADS A and B; n = 13) and a high-density group (BI-RADS C and D; n = 18). CNR was defined as $CNR = |\mu_1 - \mu_2| / \sqrt{[(\sigma_1^2 + \sigma_2^2) / 2]}$, where μ_1 and μ_2 are the mean signal intensities and σ_1 and σ_2 the standard deviations of the respective tissue regions of interest (ROI). Values are presented as mean ± standard deviation (SD). The p-value reflects the result of a paired two-sided t-test comparing PC-CT and MRI within each density subgroup. Holm p denotes the Holm–Bonferroni-corrected p-value; correction was applied across six simultaneous comparisons (three CNR tissue pairs × two breast density groups). Bold p-values indicate statistical significance after Holm correction (adjusted $p < 0.05$).

Breast density groups were classified according to BI-RADS: A = almost entirely fatty; B = scattered areas of fibroglandular tissue; C = heterogeneously dense; D = extremely dense. BI-RADS = Breast Imaging Reporting and Data System; CNR = contrast-to-noise ratio; PC-CT = photon-counting CT.

Supplemental Table 2. Detailed statistics of long- and short-axis diameters

Values are based on 31 paired target lesions measurements. Axial area product was calculated as long-axis diameter × short-axis diameter. Paired differences were calculated as MRI minus PC-CT and positive values indicate larger measurements on MRI. The 95% confidence intervals (95%-CI) refer to mean values. The p value for long-axis diameter was calculated using a paired t-test; p values for short-axis diameter and axial area product were calculated using Wilcoxon signed-rank tests because paired differences were not normally distributed.

CI = confidence interval; IQR = interquartile range; PC-CT = photon-counting CT; SD = standard deviation.

Supplemental Table 3. Paired axial target lesion size measurements on photon-counting CT (PC-CT) and MRI.

Tumor size is shown as long-axis × short-axis diameter. Differences were calculated as MRI minus PC-CT and positive values indicate larger measurements on MRI. The axial area product was calculated as long-axis diameter × short-axis diameter and is reported as a descriptive two-dimensional size surrogate, not as segmented tumor area. Long-axis categories were defined as ≤5 mm, 6–10 mm, 11–20 mm, 21–50 mm, and >50 mm. Case 13 is absent because it represents a pure DCIS case. Δ = difference; MRI = magnetic resonance imaging; PC-CT = photon-counting CT.

Supplemental Table 4. Background parenchymal enhancement (BPE) intensity in pre- and postmenopausal women for each reader.

Values are medians with interquartile ranges. Only women classified as pre- or postmenopausal are included in this subgroup table.

BPE = background parenchymal enhancement; IQR = interquartile range; MRI = magnetic resonance imaging; $PC\text{-}CT_{C+}$ = 65-keV monoenergetic post-contrast photon-counting CT reconstruction; $PC\text{-}CT_{Iodine}$ = photon-counting CT iodine-map reconstruction.

Supplemental Figures

Supplemental Figure 1. Example of ROI measurements

Representative axial contrast-enhanced photon-counting CT image showing circular regions of interest (ROI) placed in the target lesion, enhancing fibroglandular tissue and breast fat.

Declarations

Ethics approval and consent to participate:

This study was approved by the Ethics Committee of the Albert-Ludwigs-University of Freiburg, Medical Center – University of Freiburg, Faculty of Medicine, Freiburg, Germany (approval reference: EK24-1487-S1-retro; FRKS005501, retrospective). Written informed consent was not required because of the retrospective study design. The study was registered in the German Clinical Trials Register (DRKS00035784) on 20. December 2024.

Consent for publication

Not applicable. The manuscript does not contain any identifiable individual person's data

Availability of data and material

The datasets generated and/or analyzed during the current study are not publicly available due to patient privacy and institutional restrictions, but are available from the corresponding author on reasonable request and subject to applicable approvals.

Competing interests

FB has received unrestricted research grants from Siemens Healthineers and Bayer Healthcare and has served on the speaker's bureau/provided consultancy for Bayer Healthcare. All other authors declare that they have no competing interests.

Funding

This study was partially funded by the Young Researchers Grant awarded by the European Society of Breast Imaging (EUSOBI). The authors declare that no additional external funding was received for this work. The funding body had no role in the design of the study; collection, analysis, or interpretation of data; or in writing the manuscript.

Authors' contributions

CW and JN contributed equally to the conceptualization of the study. CW led data curation, formal analysis, methodology development, visualization, and writing of the original draft. She also contributed to investigation, project administration, resources, supervision, validation, software support, and manuscript review and editing. CW is the scientific guarantor of this publication. JN contributed equally to investigation, project administration, resources, supervision, validation, and conceptualization. He supported data curation, formal analysis, methodology, software implementation, visualization, and writing of the original draft. SR and JW supported

methodology and project administration. JW additionally supported resources. Both contributed to manuscript review and editing. MWB supported investigation, resources, supervision, and manuscript review and editing. FB supported project administration, resources, and manuscript review and editing. LJ, RJAD, CM, MDD, and IJB contributed to manuscript review and editing. All authors read and approved the final manuscript.

Acknowledgements

During revision, ChatGPT was used to assist with language editing, consistency checking, and formatting review. No generative artificial intelligence tool was used to create images, generate study data, perform statistical analyses, or alter scientific results. The authors reviewed and approved all artificial intelligence-assisted edits and retain full responsibility for the manuscript content.

Supplementary Files

This is a list of supplementary files associated with this preprint. Click to download.

- BMCSupplementFinal.docx